Application of a Single-Crystal CVD Diamond Detector for Fast Neutron Measurement in High Dose and Mixed Radiation Fields

メタデータ	言語: English 出版者: IEEE 公開日: 2025-01-09 キーワード (Ja): キーワード (En): Neutrons, Detectors, Radiation effects, Shape, Diamonds, Crystals, Cables, Temperature measurement, Instruments, Data acquisition 作成者: KOBAYASHI, Makoto I., YOSHIHASHI, Sachiko, OGAWA, Kunihiro, ISOBE, Mitsutaka, ASO, Tsukasa, HARA, Masanori, SANGAROON, Siriyaporn, KUSAKA, Sachie, TAMAKI, Shingo, MURATA, Isao, TOYAMA, Sho, MIWA, Misako, MATSUYAMA, Shigeo, OSAKABE, Masaki メールアドレス: 所属:
URL	http://hdl.handle.net/10655/0002000878

This work is licensed under a Creative Commons Attribution 4.0 International License.

Application of a single crystal CVD diamond detector for fast neutron measurement in high dose and mixed radiation fields

Makoto I. Kobayashi, Sachiko Yoshihashi, Kunihiro Ogawa, Mitsutaka Isobe, Tsukasa Aso, Masanori Hara, Siriyaporn Sangaroon, Sachie Kusaka, Shingo Tamaki, Isao Murata, Sho Toyama, Misako Miwa, Shigeo Matsuyama, Masaki Osakabe

***Abstract*—This paper presents the method to evaluate the fast neutron energy spectrum using the single crystal CVD diamond detector to be applicable on the radiation monitoring in advanced scientific/engineering systems usually characterized with mixed and high-dose radiation field. The pulse shape discrimination based on the shape and the width of a pulse was applied to extract events in which fast neutron hits at the specific depth of the single crystal diamond. Unfolding of the measured spectrum for extracted pulses could deduce the neutron energy spectrum. Experiments using mono-energetic neutron sources demonstrated the reliable capability of this method to evaluate the neutron energy spectrum quantitatively.**

Keywords—single crystal CVD diamond detector, neutron, pulse shape discrimination

I. INTRODUCTION

IN state-of-the-art scientific/engineering systems, such as Boron Neutron Capture Therapy (BNCT) [1-4], high-energy science [5-7], nuclear engineering [8-10], and the fusion reactor [11-14], precise neutron monitoring technology is strongly required. These systems usually operate with harsh environments characterized by high radiation field, high temperature, and very limited space for the detector.

The single-crystal diamond based detector might satisfy these criteria [15, 16]. The single-crystal diamond (SCD) is a potential material not only for radiation measurement but also power electronics, optics, material processing, and so on [17]. Recently, the manufacturing of the artificial SCD has been developed using chemical vapor deposition (CVD) processes, and the detector-grade SCD has been fabricated [18]. The single-crystal CVD diamond detectors (SDD) assembled with detector-grade SCDs are commercially available.

The properties of SCD are reviewed in reference [19]. The size of the detector-grade SCD is quite small [20], usually less than 10 cm^3 including the detector housing. Some studies have revealed that the detection efficiency of SDD for 14 MeV neutrons remains steady up to a neutron fluence of approximately 0.5×10^{14} n cm^{-2} [21]. Additionally, the high-temperature tolerance of SDD in neutron measurement under 473 K has been demonstrated [22]. These excellent properties of SDD should enable neutron measurement under harsh environments in advanced systems.

For example, due to its high radiation tolerance and compact size, continuous radiation dose monitoring on the body of a patient can be possible in BNCT. It's worth emphasizing that the effective Z of SCD, close to the constitutional atoms of the human body, enables a tissue-equivalent X-ray dose monitoring during therapy [23]. The SDD can be placed in a narrow space due to its compact size. We can transport the SDD through a narrow port into the intense radiation field, avoiding high-level occupational exposure. This is a significant advantage in radiation monitoring during the decommissioning of damaged nuclear power plants such as the Fukushima-Daiichi nuclear power station [24, 25], where the space to transport the radiation monitor is limited and the radiation level is extremely high. Additionally, it is worth emphasizing that the compact size of the SDD enables radiation field evaluation with minimal modification of the radiation field due to the detector.

Furthermore, SDD so far has been the only accepted solution

Manuscript received XX; revised XX; accepted XX. Date of publication XX; date of current version XX. This work is supported by the NINS program for cross-disciplinary study (Grant number 0131190). This work is also performed with the support and under the auspices of the NIFS Collaboration Research program (NIFS19KOAA001, NIFS19KLPA001), and LHD project budget.

Makoto I. Kobayashi is with the National Institute for Fusion Science, Toki 509-5292, Japan, and also with the Graduate University for Advanced Studies, SOKENDAI, Toki 509-5292, Japan (e-mail: kobayashi.makoto@nifs.ac.jp).

Sachiko Yoshihashi is with Nagoya University, Nagoya, Japan (e-mail: s-yoshihashi@energy.nagoya-u.ac.jp).

Kunihiro Ogawa, Mitsutaka Isobe and Masaki Osakabe are with the National Institute for Fusion Science, Toki 509-5292, Japan, and also with the Graduate University for Advanced Studies, SOKENDAI, Toki 509-5292, Japan (e-mail: ogawa.kunihiro@nifs.ac.jp; isobe.mitsutaka@nifs.ac.jp; osakabe.masaki@ac.jp).

Tsukasa Aso is with the National Institute of Technology, Toyama College, Toyama, Japan (e-mail: aso@nc-toyama.ac.jp).

Masanori Hara is with the University of Toyama, Toyama, Japan (e-mail: masahara@ctg.u-toyama.ac.jp).

Siriyaporn Sangaroon is with the Mahasarakham University, Maha Sarakham, Thailand (e-mail:siriyaporn.s@msu.ac.th).

Sachie Kusaka, Shingo Tamaki and Isao Murata are with the Osaka University, Suita, Japan (e-mail: kusaka@see.eng.osaka-u.ac.jp; tamaki@see.eng.osaka-u.ac.jp; murata@see.eng.osaka-u.ac.jp).

Sho Toyama, Misako Miwa, and Shigeo Matsuyama are with the Tohoku University, Sendai, Japan (e-mail; sho.toyama.a3@tohoku.ac.jp; misako.miwa.c7@tohoku.ac.jp; shigeo.matsuyama.a5@tohoku.ac.jp).

for diagnostics of tritium breeding rate and fast neutron flux in the harsh environments in the blanket of a fusion reactor, where high temperature and high radiation dose are expected, and the ports for diagnostics are limited.

Our previous study proposed to apply only one SDD with the Pulse Shape Discrimination (PSD) technique on the monitoring for the tritium breeding rate and the fast neutron flux in the breeding blanket of fusion reactor [26]. With that method, the influence of gamma-ray, which, in this case, are always associated with neutrons, could be eliminated. Then, the discriminative measurement for nuclear reaction products including recoil tritium from the thin lithium fluoride foil under fast neutron irradiation was demonstrated. Simultaneously, the energy deposition spectrum induced only by fast neutrons could be obtained, although the processes to convert the energy deposition spectrum to the neutron energy spectrum combined with this PSD method has not been completed yet. The study presented herein is a continuation where we demonstrate the neutron energy spectrum reconstruction through PSD processing. For this demonstration, mono-energetic neutrons sources were used. The unfolding of the energy deposition spectrum was conducted to obtain the neutron energy spectrum according to the response matrix of the SDD for fast neutrons evaluated by Geant4 simulation [27].

II. EXPERIMENTAL

A. 14.1 MeV neutron irradiation

14.1 MeV neutron irradiation was carried out at OKTAVIAN facility of Osaka University [28]. In this neutron source, the tritium target consisted of tritium atoms stored in titanium thin layer deposited on copper substrate was placed in front of deuteron beam direction to produce fast neutron through ^{3}H(d,n)^{4}He reaction.

The SDD was B-12 Knof diamond detector manufactured by Cividec instrumentation GmbH [29]. The active area and the thickness of the SCD in this detector was 4 × 4 mm^2, and 0.5 mm, respectively. A 100 nm-thick titanium electrode was deposited on both surfaces of the SCD. The SDD was placed with the 90-degree angle to the deuteron beam direction to be exposed to 14.1 MeV mono-energetic neutrons, at 130 mm away from the center of the tritium target. The energy of deuteron was 300 keV. The schematic drawing of the experimental set-up is given in Fig. 1 (a).

B.5.5 MeV neutron irradiation

In the second experiment, 5.5 MeV neutron irradiation was performed at the Fast Neutron Laboratory (FNL) of Tohoku University [30]. In this facility, the dynamitron accelerator produces a 3 MeV deuteron beam with a current of approximately 0.5 μA. The target used in this irradiation was the deuterium-gas target consisting of a gas-cell filled with deuterium gas with the pressure of near 1 atm. The gas-cell has a 6.47 μm thick Haver foil window. The energetic deuterons can penetrate this window into the gas-cell to produce neutrons through ^{2}H(d, n)^{3}He reaction.

The SDD in this experiment was a B-6 high-temperature thermal neutron detector manufactured by Cividec instrumentation GmbH [29]. In this detector, the SCD, with the same active area and thickness as in detector model B-12, is contained in a housing made of polyether ether ketone (PEEK). In the conventional use of this detector, the SCD is faced to a thin lithium fluoride layer deposited on the lid to produce nuclear reaction products by ^{6}Li(n,α)^{3}H reaction. In this work, however, the lid was taken out to open the SCD surface to fast neutrons. Considering the energy loss of 3 MeV deuterons in the Haver foil and the 0-degree angle between the deuteron beam and the SDD, the mono-energetic 5.5 MeV neutrons can be irradiated into the SCD [31]. The distance between the SCD and the end of the gas target was 20 mm. The schematic drawing of the experimental set-up is also given in Fig. 1 (b)

C. DAQ systems

In the above neutron irradiation experiments, the same electronic instruments were used as drawn in Fig. 1 (c). The data acquisition (DAQ) system (Techno AP APV8102-14MWPSAGb) used here consists of a fast-processing analog to digital converter (ADC) and a field programmable gate array (FPGA) with a sampling rate of 1 GHz and a 14 bit resolution [32]. The pre-amplifier (CIVIDEC C2-HV broadband amplifier) directly connected to the SDD and powered by a +12 V DC power supply (Matsusada Precision PLD-18-2). This pre-amplifier is to apply +250 V on the electrode of the SDD from a high voltage power supply (ORTEC 428), and to amplify the signals from the SDD to send them to the DAQ system. These instruments were connected by co-axial cables. In the experiments conducted at FNL the cable lengths were 10 m. Longer cables were needed at OKTAVIAN to reach the instruments placed outside of the irradiation room to avoid the intense neutron field.

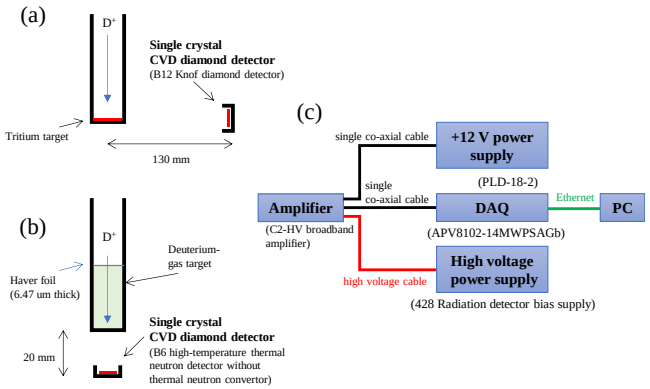

Fig. 1. The schematic drawing of (a) detector layout in 14.1 MeV neutron irradiation, (b) detector layout in 5.5 MeV neutron irradiation, (c) layout of electronic components used in both experiments.

III. SIMULATIONS

A. Neutron transport calculation in OKTAVIAN facility using MCNP6

Neutron transport calculation in OKTAVIAN facility was conducted using the general Monte Carlo N-Particle code (MCNP6) [33]. The ENDF/B-VII.1 Evaluated Nuclear Data Library was used in this calculation [34]. The vacuum components, tritium target, coolant channel as well as the irradiation room was modeled. The angular distributions of neutron energy and flux at the target were the same as that validated at Fusion Neutron Source (FNS) of JAEA, because the OKTAVIAN employed the same target system as that in FNS [35]. The neutron energy spectrum at the position of the SDD was estimated using the neutron transport probability obtained by this calculation and the actual neutron yield in the experiment measured by a fission chamber placed around the tritium target.

B. Neutron transport calculation in FNL using PHITS

Neutron transport calculation in FNL facility was conducted using Particle and Heavy Ion Transport code System (PHITS) [36]. For this calculation, the gas target was modeled. The 3.0 MeV deuteron beam was also set to calculate the transport of deuteron in the Haver foil and the gas-cell, and to estimate the subsequent neutron generation and transport. The Frag Data Table of ^{2}H(d,n)^{3}He reaction was applied to calculate the total and angular neutron yield. The details of this calculation can be found elsewhere [31]. The neutron energy spectrum at the position of the SDD was estimated according to this calculation and the deuteron beam current in the experiment.

C. Neutron energy deposition into the SCD by Geant4

Energy deposition spectrum by the hit of fast neutrons into the SCD was estimated using Geant4-based application templet (Galet [37]). In the simulation, mono-energetic neutron was set as the source, and the energy deposition in each event was integrated. We used ENDF/B-VII.1 Evaluated Nuclear Data Library [34] and FTFP_BERT_HP physics model for modeling recoil carbon atoms in the SCD [27]. Also, we applied NRESP7.1 model to use multistep breakup model for ^{12}C(n,$n'2\alpha$)α reaction [38, 39].

The energy deposition spectra in each mono-energetic neutron irradiation were evaluated in the neutron energy range of 0.3-15.0 MeV with the energy interval of 0.3 MeV. The energy dispersion was set to 5% throughout the energy range. The energy deposition efficiencies in each energy bin (0.3 MeV interval, from 0.3 MeV to 15.0 MeV) with respect to the fast neutron energy (0.3 MeV interval, from 0.3 MeV to 15.0 MeV) were compiled as a response matrix of the SCD for fast neutrons.

IV. ANALYSES

A. Pulse shape discrimination

The pulse in the SDD is induced by the drift of electron-hole pairs in the SCD, therefore, the shape of the pulse depends on the initial depth distribution of electron-hole pairs [40, 41]. Due to the sensitivity of the SCD to various particles such as energetic ions, gamma-rays and neutrons, several pulse shapes can be obtained in the SDD in the mixed radiation field.

Fast neutrons can induce electron-hole pairs as point-like throughout the entire bulk of the SCD. In particular, pulses with a rectangular shape and a narrow pulse width can be found in fast neutron irradiation due to events at the specific depth of the SCD where the drift durations of electrons and holes are equivalent. This specific depth of the SCD is usually called the ballistic center region (BCR), and these events can be induced only by fast neutrons [42, 43]. Therefore, the fast neutron measurement is possible by the extraction of BCR pulses even under mixed radiation field.

The PSD method applied in this work extracted these narrow rectangular shaped pulses induced only by fast neutrons, using rectangularity *(R)* and the FW1/4PH (Full Width of One-Fourth of the Peak Height) of each pulse. R is defined as $R = 4Q/3AW$, where A, W, Q indicate the peak height, FW1/4PH, and the charge integral exceeding $A/4$, respectively. R reaches unity when the shape of the pulse is close to the rectangular shape. According to our previous study, pulses with $R > 0.63$ and 5 ns $< W <$ 6.5 ns were extracted as events occurred at the BCR from fast neutron interactions. The histogram of the total charge of these pulses were converted into the energy deposition spectrum using the alpha particle source of ^{241}Am. The detail of these PSD processing can be found in Ref. [44, 45].

Figure 2 (a) shows typical shapes of pulses obtained under 14.1 MeV neutron irradiation before the PSD. Various shapes of pulses indicate that events which induced these pulses might occur at different depths of the SCD. Also, the deposition energy from a neutron to the SCD should be different for each event, resulting in various total charges of these pulses. The W distribution of pulses in the 14.1 MeV neutron irradiation experiments before the PSD can be found as a black line in Fig. 3. The values of W are widely distributed from 3 ns to above 19 ns.

Pulse shapes of pulses extracted by the PSD are displayed in Fig. 2 (b). Pulses with narrow widths and closely rectangular shapes were successfully extracted. The W distribution of these pulses is added as a red line in Fig. 3. The W of extracted pulses ranges from 5 to 6.5 ns. The decrease in the count number in this region after the PSD is due to the filter by R.

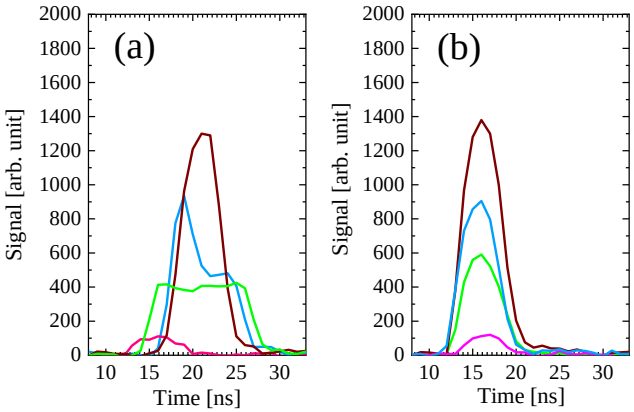

Fig. 2. Examples of pulse shapes measured during 14.1 MeV neutron irradiation (a) before the PSD processing (b) after the PSD processing.

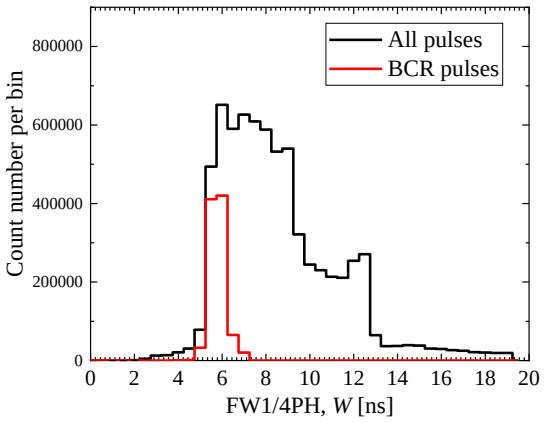

Fig. 3. The FW1/4PH (W) distributions of all pulses and BCR pulses measured during 14.1 MeV neutron irradiation experiment. The number of pulses analyzed here is ~6.9 × 10^6.

It should be noted that a large portion of pulses are excluded by the PSD (please compare the area of the black line and the red line in Fig. 3). The degradation in the statistical accuracy of fast neutron measurement is a typical drawback of this method, and should be considered when designing the measurement.

B. Evaluation of neutron energy spectrum

The neutron energy spectrum was evaluated from the energy deposition spectrum of BCR pulses. The energy deposition spectrum can be expressed as follows.

$$\Psi_i = \frac{\omega_i}{\theta}\sum_{j=1}^{N} P_{i,j}\,\phi_j \quad (1)$$

Here, Ψ, ω, θ, P, ϕ indicate the energy deposition rate [s^{-1}], noise-cut function, the overall PSD efficiency, response matrix, and the number of incident neutrons into the SCD [s^{-1}], respectively. The subscript i indicates the deposition energy bin number, which ranges from 0.3 to 15.0 MeV with an interval of 0.3 MeV, resulting in a total 50 bins (N = 50). The subscript j denotes the index number of fast neutron energy in the Geant4 simulation, also ranging from 0.3 to 15.0 MeV with an interval of 0.3 MeV, resulting in a total of 50 indices (M = 50). The detail description of Eq. (1) can be given by Eq. (2).

$$\begin{bmatrix}\Psi_1\\ \Psi_2\\ \vdots\\ \Psi_i\\ \vdots\\ \Psi_{N-1}\\ \Psi_N\end{bmatrix} = \frac{\omega_i}{\theta}\begin{bmatrix} P_{1,1} & P_{1,2} & \cdots & P_{1,j} & \cdots & P_{1,M-1} & P_{1,M}\\ P_{2,1} & P_{2,2} & & \vdots & & P_{2,M-1} & P_{2,M}\\ \vdots & & \ddots & & \ddots & & \vdots\\ P_{i,1} & \cdots & & P_{i,j} & & \cdots & P_{i,M}\\ \vdots & & & & \ddots & & \vdots\\ P_{N-1,1} & P_{N-1,2} & \ddots & \vdots & & P_{N-1,M-1} & P_{N-1,M}\\ P_{N,1} & P_{N,2} & \cdots & P_{N,j} & \cdots & P_{N,M-1} & P_{N,M}\end{bmatrix}\begin{bmatrix}\phi_1\\ \phi_2\\ \vdots\\ \phi_j\\ \vdots\\ \phi_{M-1}\\ \phi_M\end{bmatrix} \quad (2)$$

$P_{i,j}$ indicates the energy deposition efficiency of the SCD at the i-th deposition energy bin by neutron irradiation with the energy of 0.3j MeV. Therefore, the energy deposition rate at the i-th deposition energy bin can be expressed as follows:

$$\Psi_i = \frac{\omega_i}{\theta}\left(P_{i,1}\phi_1 + P_{i,2}\phi_2 + \cdots + P_{i,j}\phi_j + \cdots + P_{i,M-1}\phi_{M-1} + P_{i,M}\phi_M\right) \quad (3)$$

The energy deposition efficiencies in each deposition energy bin by j-th mono-energetic neutron irradiation $\left(P_{1,j},\ P_{2,j}, \cdots P_{i,j}, \cdots, P_{N-1,j}, P_{N,j}\right)$ can be evaluated in a single run of Geant4 simulation. Therefore, energy deposition efficiencies in each deposition energy bin, evaluated by a single run of Geant4 simulation changing irradiated neutron energies from 0.3 to 15 MeV (50 runs in total) were compiled to make a response matrix of the SCD for neutrons in the neutron energy range up to 15 MeV. Note that because the Q-values of interactions between neutrons and the SCD are less than or equal to 0 (see Section V), P in the region $i \geq j$ should be 0. Accordingly, the lower triangular portion excluding the diagonal component in the response matrix can be filled with 0.

The overall PSD efficiency was defined to the ratio of BCR pulse count to overall pulse count. The noise-cut function was applied to reshape the response matrix to take care the influence of current threshold in DAQ system set for noise cutting, which is ignored in Geant4 simulation. The following sigmoid-like function was assumed for this function.

$$\omega_i = 2^{\beta}\left(\frac{1}{1+e^{-\alpha\gamma i}} - \frac{1}{2}\right)^{\beta} \quad (4)$$

Parameters of α, β were selected so that the energy deposition spectrum for 14.1 MeV neutrons estimated in Geant4 simulation reproduces the actual spectrum in the measurement. The detail of these parameters is discussed in Fig. 5 below. The parameter γ indicates the interval in the energy bin which is 0.3 MeV here.

To estimate the number of incident neutrons, ϕ, the Newton-Raphson method was used. First, the equation (1) was modified as follows.

$$f_i = \Psi_i - \frac{\omega_i}{\theta}\sum_{j=1}^{N} P_{i,j}\,\phi_j \quad (5)$$

Here, f indicates the residual of equation (1). Then, following iterative calculation was done to decrease f.

$$\boldsymbol{\phi}^{(k+1)} = \boldsymbol{\phi}^{(k)} - \left[\frac{\partial \boldsymbol{f}}{\partial \boldsymbol{\phi}}\right]^{-1}\boldsymbol{f} \quad (6)$$

The superscript (k) indicates the step number of iterative calculation. The iteration of equation (6) replacing ϕ finished when the following condition was achieved in all energy bins.

$$\left|\frac{\boldsymbol{\phi}^{(k+1)} - \boldsymbol{\phi}^{(k)}}{\boldsymbol{\phi}^{(k)}}\right| = 10^{-10} \quad (7)$$

Accordingly, the number of incident neutrons can be obtained. These processes need the first guess in the number of incident neutrons. In this study, $\boldsymbol{\phi}$ = 1 was set, thus any expectation in neutron energy spectrum was not used.

V. RESULTS AND DISCUSSION

Figure 4(a) and (b) show each energy deposition spectrum of all pulses in 14.1 MeV and 5.5 MeV neutron irradiation experiments. The energy deposition spectra of BCR pulses obtained by PSD processing are also displayed. The results indicated that there are various peaks in the case of 14.1 MeV neutron irradiation although 5.5 MeV neutron irradiation resulted in a peak in lower deposition energy region. Even a significant decrease in count by PSD processing, the shape of the energy deposition spectra of BCR pulses hardly changed compared to those of all pulses in both neutron irradiation experiments. However, the evidence of a successful discrimination applied in this work can be found in the spectrum above the deposition energy of 3 MeV for 5.5 MeV neutron irradiation. As an example, the inset in Fig. 4(b) depicts

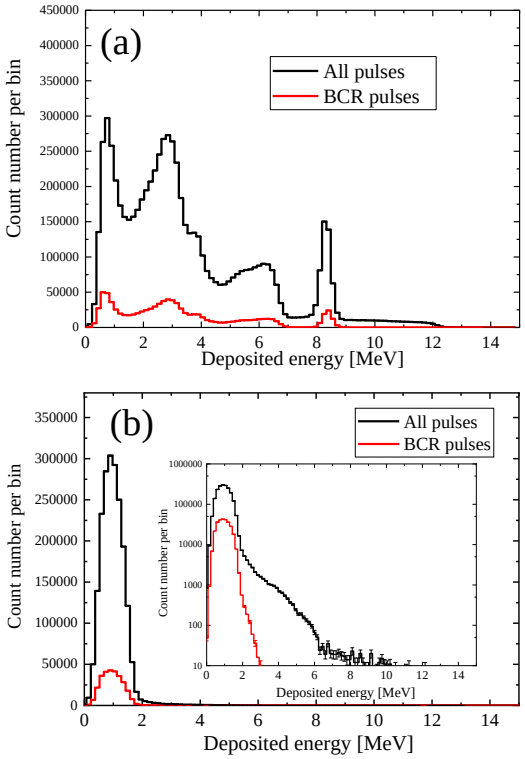

Fig. 4. The energy deposition spectra of all pulses and BCR pulses in (a)14.1 MeV neutron irradiation experiment, and (b)5.5 MeV neutron irradiation experiment. The results of 5.5 MeV neutron irradiation experiment with log-scale for y-axis is added in Fig. 4(b) as an example to show the successful PSD processing. The number of all pulses in each spectrum were ~6.9×10^6 and ~2.0×10^6, respectively.

the energy deposition spectrum with log-scale in y-axis. The energy deposition above 3 MeV, which would be induced by recoil protons from housing at the surface region of the SCD, was completely rejected by the PSD processing.

The overall PSD efficiency was evaluated to be 0.135 ± 0.04 from the results of 14.1 MeV neutron irradiation experiment. This value was also used in the evaluation of neutron energy spectrum in 5.5 MeV neutron irradiation experiment.

The energy deposition spectrum of BCR pulses, the estimated deposition spectrum by Geant4 and the estimated deposition spectrum multiplied by the noise-cut function for the case of 14.1 MeV neutron irradiation are compared in Fig. 5. According to some literatures, peaks around 8.4 MeV, 6 MeV, 3 MeV were assigned to the energy deposition events of energetic ions produced by $^{12}C(n,\alpha)^9Be$ (Q ~ -5.702 MeV), $^{12}C(n,n2\alpha)\alpha$ (Q ~ -7.275 MeV) and $^{12}C(n,n')^{12}C$ (Q ~ 0 MeV) reactions, respectively [19, 43, 46].

The estimated energy deposition spectrum by Geant4 was quite comparable to the actual energy deposition spectrum. However, a slight difference can be found in the peak by $^{12}C(n,n')^{12}C$ around 3 MeV, and there was a significant difference in lower energy region blow 1 MeV. The Geant4 simulation ignored the current threshold in the DAQ system for noise-cutting, thus a significant difference in lower energy region emerged. The estimated energy deposition spectrum

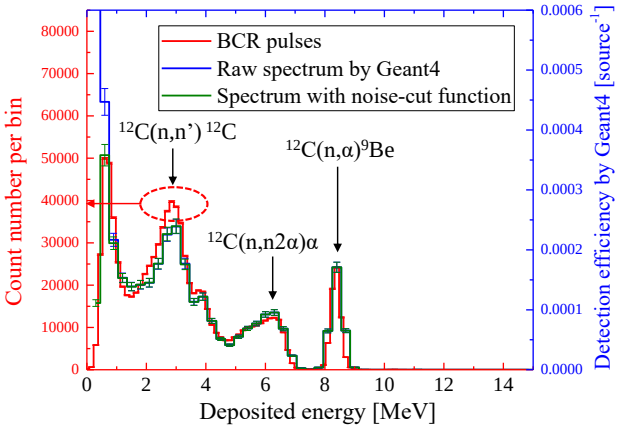

Fig. 5. The energy deposition spectra of BCR pulses in 14.1 MeV neutron irradiation experiment (red line), the estimated spectra obtained by Geant4 simulation (blue line), and the estimated spectra by Geant4 multiplied with noise-cut function (green line). The parameters of α, β in this function were 7.5 and 10, respectively.

multiplied with the noise-cut function displayed in this figure successfully reproduced the actual energy deposition spectrum below 1 MeV. In the following calculation, the same values in parameters of α, β in noise-cutting function were applied on all energy deposition spectra estimated by Geant4 with various incident neutron energies.

According to the results in Figs. 4 and 5, θ and ω were deduced, respectively. Then, the neutron energy spectra for 14.1 MeV neutron irradiation and 5.5 MeV neutron irradiation experiments were evaluated. Figure 6 summarizes the results of these evaluation. The deduced neutron energy spectrum for 14.1 MeV neutron irradiation experiments was compared to that estimated by transport simulations using MCNP6 in Fig. 6(b).

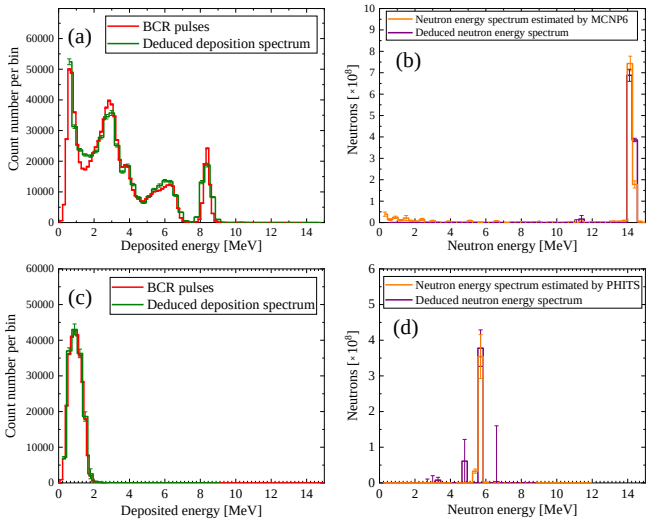

Fig. 6. The results of neutron energy spectrum evaluation. (a) the comparison of the energy deposition spectra of BCR pulses to the estimated deposition spectrum in 14.1 MeV neutron irradiation experiment, (b) the comparison of the deduced neutron energy spectra to that estimated by MCNP6. The respective results are displayed in (c) and (d) for 5.5 MeV neutron irradiation experiment.

Also, the estimated energy deposition spectrum by the deduced neutron energy spectrum is compared to the actual energy deposition spectrum with PSD processing in Fig. 6(a). The same series of results for 5.5 MeV neutron irradiation experiment are displayed in Figs. 6 (c) and (d). First, the estimated energy deposition spectra for both cases were quite comparable to the actual energy deposition spectra quantitatively. Even though there are small peaks in the deduced neutron energy spectra, which might be caused by a discrepancy in the cross-section library used in Geant4 simulation, it can be fairly recognized that the deduced neutron energy spectra were quantitatively consistent with the estimated spectra by MCNP6 or PHITS simulations.

VI. Conclusion

In this study, we demonstrated the evaluation of neutron energy spectrum combined with the PSD processing to extract pulses induced only by fast neutrons in the SDD. This method has processes to reject pulses induced by gamma-rays and energetic ions in PSD processing, and showed reliable capability to evaluate the neutron energy spectrum quantitatively. Accordingly, the developed method here opened to measure fast neutrons in mix radiation field.

On the other hand, there are still challenges in applying this method to various environments. For example, it has been reported that the width of pulses in the SDD can increase with rising detector temperature [47]. Since the current PSD method relies on pulse width to extract BCR pulses, this broadening can affect the likelihood of exceeding the current threshold in the DAQ system. Therefore, the PSD method should be optimized as a function of detector temperature before applying it to systems operating at higher temperatures.

References

[1] "Current status of Neutron Capture Therapy", IAEA-TECDOC-1223, 2001.

[2] "Advances in Boron Neutron Capture Therapy", IAEA, 2023.

[3] X. Cheng, F. Li, L. Liang, "Boron Neutron Capture Therapy: Clinical Application and Research Progress", *Curr. Oncol.*, vol. 29, no. 10, pp. 7868-7886, Oct. 2022.

[4] A.H. Soloway, W. Tjarks, B.A. Barnum, F.-G. Rong, R.F. Barth, I.M. Codogni, and J.G. Wilson, "The Chemistry of Neutron Capture Therapy" *Chem. Rev*. vol. 98, no. 4, pp. 1515–1562, May. 1998.

[5] P.K. Sarkar, "Neutron dosimetry in the particle accelerator environment", Radiat. Meas. Vol. 45, no. 10, pp. 1476-1483, Dec. 2010.

[6] V. Blideanu, C. Besnard-Vauterin, D. Horváth, B. Lefebvre, F. Salvat-Pujol, R. Versaci, Neutron spectra from photonuclear reactions: Performance testing of Monte-Carlo particle transport simulation codes, *Nucl. Instrum. Methods Phys. Res. B*, vol. 549, Art. no. 165292, Feb. 2024.

[7] N. Colonna, F. Gunsing, F. Käppeler, "Neutron physics with accelerators", *Prog. Part. Nucl. Phys.*, vol. 101 pp. 177-203, Jul. 2018.

[8] V. Verma, P. Filliatre, C. Hellesen, S. Jacobsson Svärd, C. Jammes, "Neutron flux monitoring with in-vessel fission chambers to detect an inadvertent control rod withdrawal in a sodium-cooled fast reactor", *Ann. Nucl. Energy*, vol. 94, pp. 487-493, Aug. 2016.

[9] Y.-G Li, Y.-Q Shi, Y.-B Zhang, P Xia, "Reactor fission rate measurement for miniature neutron source reactor by solid state nuclear track detector", *Radiat. Meas.*, vol. 34, pp. 589-591, Jun. 2001.

[10] N.A.Z. Kamarudin, A.F. Ismail, M.H. Rabir, K.Kok Siong, "Neutronic optimization of thorium-based fuel configurations for minimizing slightly used nuclear fuel and radiotoxicity in small modular reactors", *Nucl. Eng. Technol*., available online, Feb. 2024.

[11] M. Pillon, M. Angelone, P. Batistoni, R. Villari, S. Almaviva, M. Marinelli, E. Milani, G. Prestopino, C. Verona, G. Verona Rinati, "Development of on-line tritium monitor based upon artificial diamond for fusion applications", I*EEE Trans. Nucl. Sci*,. vol. 58, no. 3, pp. 1141, May. 2011.

[12] M. Angelone, N. Fonnesu, A. Colangeli, F. Moro, M. Pillon, R. Villari, "Calibration and test of a ^{6}LiF-diamond detector for the HCPB mock-up experiment at JET", *Fus. Eng. Des*. Vol. 146, pp. 1755-1758, Sep. 2019.

[13] M. Angelone, D. Lattanzi, M. Pillon, M. Marinelli, E. Milani, A. Tucciarone, G. Verona-Rinati, S. Popovichev, R.M. Montereali, M.A. Vincenti, A. Murari, JET-EFDA Contributors, "Development of single crystal diamond neutron detectors and test at JET tokamak", *Nucl. Instrum. Meth. in Phys. Res. A*, Vol. 595, pp. 616-622, Oct. 2008.

[14] T. Du, X. Peng, Z. Chen, Z. Hu, L. Ge, L. Hu, G. Zhong, N. Pu, J. Chen, T. Fan, "Time Dependent DD Neutrons Measurement Using a Single Crystal Chemical Vapor Deposition Diamond Detector on EAST", *Plasma Sci. Technol*., Vol. 18, pp. 950-953, Sep. 2016.

[15] S. Koizumi,C. Nebel, M. Nesladek, "Physics and Applications of CVD Diamond", Wiley‐VCH Verlag GmbH & Co. KGaA, 2008.

[16] C.E. Nebel, "Electronic properties of CVD diamond", *Semicond. Sci. Technol*. Vol. 18, S1, Feb. 2003.

[17] U.F. Ahmad, Y.S Wudil, A. Imam, N.F. Isa, M.A. Gondal., M.A. Al-Osta, "Applications of carbon-based diamond detectors: A critical review", *Mater. Today Commun.*, Vol. 36, Art. no. 106409, Aug. 2023.

[18] M. Schwander, K. Partes, "A review of diamond synthesis by CVD processes", *Diam. Relat. Mater*. Vol. 20, pp. 1287-1301, Oct. 2011.

[19] M. Angelone and C. Verona, "Properties of Diamond-Based Neutron Detectors Operated in Harsh Environments", *J. Nucl. Eng.*, Vol. 2 pp. 422-470, Oct. 2021.

[20] M. Sasao, T. Nishitani, A. Krasilnilov, S. Popovichev, V. Kiptily, J. Kallne, "Fusion Product Diagnostics", *Fusion Sci. Technol*., Vol. 53, pp. 604-639, Feb. 2008.

[21] M. Passeri, F. Pompili, B. Esposito, M. Pillon, M. Angelone, D. Marocco, G. Pagano, S. Podda, M. Riva, "Assessment of single crystal diamond detector radiation hardness to 14 MeV neutrons", *Nucl. Instrum. Methods Phys. Res., A*, Vol. 1010, Art. no. 165574, Sep. 2021.

[22] O. Philip, F. Gicquel, V. Ernst, Z. Zhou, "Development and Test of a Diamond-Based Fast Neutron Detector for 200 °C Operation", *IEEE Trans. Nucl. Sci.*, Vol. 64, pp. 2683-2689, Aug. 2017.

[23] M. Jung, Ph. Meyer, J. Morel, C. Teissier, P. Siffert, "Diamond X-ray personal dosimetry. Numerical evaluation against silicon response", *Nucl.Instrum.Meth.A*, Vol. 511, pp. 417-424, Oct. 2003.

[24] K. Terashima, K. Okumura, "A Prediction Method for the Dose Rate of Fuel Debris Depending on the Constituent Elements", *J. Adv. Simulat. Sci. Eng*. Vol. 8, no. 1, pp. 73-86, Mar. 2021.

[25] Y. Terasaka, Yuki Sato, Akira Uritani, "First demonstration of a single-end readout position-sensitive optical fiber radiation sensor inside the Fukushima Daiichi Nuclear Power Station based on wavelength-resolving analysis", *Nucl. Instrum. Methods Phys. Res. A*, Vol. 1062, Art. no. 169227, May 2024.

[26] M.I. Kobayashi, et al., "Measurement of 6Li burn-up reaction rate using a single crystal CVD diamond detector under fast neutron irradiation environment", *Fusion Eng. Des.*, Vol. 193, Art. no. 113799, Aug. 2023.

[27] S. Agostinelli, et al., "Geant4 – a simulation toolkit", *Nucl. Instrum. Meth. A*, Vol. 506, pp. 250-303, Jul. 2003.

[28] H. Sakane, et al., "Measurement of activation cross-sections of (n, np+d) reactions producing short-lived nuclei in the energy range between 13.4 and 14.9 MeV using an intense neutron source OKTAVIAN", *Annals of Nucl. Energy*, Vol. 29, no. 1, pp. 53-66, Jan. 2002.

[29] https://cividec.at

[30] S. Matsuyama, et al., "Improvement and recent applications of the Tohoku microbeam system", *Nucl. Instrum. Meth. Phys. Res. B*, Vol. 318A, no. 1, pp. 32-36, Jan. 2014.

[31] T. Nishitani, S. Yoshihashi, K. Ogawa, M. Miwa, S. Matsuyama, A. Uritani, "Neutron yield calculation of thin and thick d-D targets by using PHITS with frag data table", *J. Nucl. Sci. Technol.*, Vol. 59, no. 4, pp. 534-541, Oct. 2022.

[32] K. Ogawa, M. Isobe, T. Nishitani, T. Kobuchi, "The large helical device vertical neutron camera operating in the MHz counting rate range", *Rev. Sci. Instrum*., Vol. 89, Art. no. 113509, Nov. 2018.

[33] D.B. Pelowits, "MCNP6 User's Manual", LA-CP-13-00634, Los Alamos National Laboratory, 2013.

[34] ENDF/B-VII.1 Evaluated Nuclear Data Library, Brookhaven National Laboratory.

[35] C. Konno, M. Ohta, K. Takakura, K. Ochiai, S. Sato, "FENDL-3 benchmark test with neutronics experiments related to fusion in Japan", *Fusion Eng. Des.*, Vol. 89 no. 9-10, pp. 1889-1893, Oct. 2014.
[36] T. Sato, et al., "Features of Particle and Heavy Ion Transport code System (PHITS) version 3.02", *J. Nucl. Sci. Technol.*, Vol. 55, pp. 684-690, Jan. 2018.
[37] T. Aso, W. Takase, T. Sasaki, "Galet – Geant4 based application templet for primers", Trans. GIGAKU, Vol. 6, Apr. 2019.
[38] V.V. Gaganov, et al., "Experimental characterisation of diamond-based neutron spectrometer", *J. Instrum*, Vol. 17 Art. no. T09001, Sep. 2022.
[39] S. A. Kuvin, et al., "Validation of neutron-induced reactions on natural carbon using an active target at neutron energies up to 22 MeV at LANSCE", *Phys. Rev. C* Vol. 104, Art. no. 014603, Jul. 2021.
[40] W. Shockley, "Currents to Conductors Induced by a Moving Point Charge", *J. Appl. Phys.*, Vol. 9, pp. 635-636, Oct. 1938.
[41] Z. He., "Review of the Shockley–Ramo theorem and its application in semiconductor gamma-ray detectors", *Nucl. Instrum. Methods Phys. Res. A*, Vol. 463, no. 1-2, pp. 250-267, May 2001.
[42] P. Kavrigin, P. Finocchiaro, E. Griesmayer, E. Jericha, A. Pappalardo and C. Weiss, "Pulse-shape analysis for gamma background rejection in thermalneutron radiation using CVD diamond detectors", *Nucl. Instrum. Methods Phys. Res. A*, Vol. 795, pp. 88-91, Sep. 2015.
[43] C. Weiss, H. Frais-Kolbl, E. Griesmayer and P. Kavrigin, "Ionization signals from diamond detectors in fast-neutron fields", *Eur. Phys. J. A*, Vol. 52, Art. no. 269, Sep. 2016.
[44] M.I. Kobayashi, et al., "A comprehensive evaluation of the thermal neutron detection efficiency by a single crystal CVD diamond detector with a LiF thermal neutron converter", *Fusion Eng. Des.*, Vol. 179, Art. no. 113117, Jun. 2022.
[45] M.I. Kobayashi, et al., "Thermal Neutron Measurement Capability of a Single Crystal CVD Diamond Detector near the Reactor Core Region of UTR-KINKI", *Plasma Fusion Res.*, Vol. 17, Art. no. 2405045, Jun. 2022.
[46] J. Liu, et al., "Simultaneous measurement of energy spectrum and fuence of neutrons using a diamond detector", *Sci. Rep.*, Vol. 12, Art. no. 12022 Jul. 2022.
[47] B. Kraus, et al., "Charge carrier properties of single-crystal CVD diamond up to 473 K," Nucl. Instrum. *Meth. Phys. A*, Vol. 989 Art. No. 164947 Feb. 2021.

Makoto I. Kobayashi was born in Fujinomiya, Shizuoka, Japan, in 1986. He received the Ph.D. degree in science from Shizuoka University, Shizuoka, Japan, in 2014. He worked in the Shizuoka prefectural government for environmental radiation research from 2014 to 2016. He has been an Assistant Professor with the National Institute for Fusion Science, Toki, Japan, since 2016. His current research interests include tritium and radiation transports in fusion systems.

Sachiko Yoshihashi, photograph and biography not available at the time of publication.

Kunihiro Ogawa was born in Mino, Gifu, Japan, in 1984. He received the M.S. and Ph.D. degrees from the Department of Energy Science and Engineering, Nagoya University, Nagoya, Japan, in 2008 and 2011, respectively. He studied electrical and electronic engineering at Ritsumeikan University, Kyoto, Japan, from 2003 to 2006. He has been with the National Institute for Fusion Science, Toki, Japan, since 2012. He has been an Associate Professor with the National Institute for Fusion Science since 2020. His current research interests include the energetic ion confinement in magnetically confined fusion plasmas.

Mitsutaka Isobe was born in Nagoya, Aichi, Japan, in 1967. He received the B.S. and M.S. degrees in applied physics from Fukui University, Fukui, Japan, in 1991 and 1993, respectively, and the Ph.D. degree in fusion science from the Graduate University for Advanced Studies, SOKENDAI, Hayama, Japan, in 1996. He had been involved in a compact helical system project from 1997 to 2006 and is currently involved in a large helical device (LHD) project. He has been a Professor with the National Institute for Fusion Science, Toki, Japan, since 2015. His current research interests include the confinement study of energetic ions by means of neutron diagnostics in magnetically confined fusion plasmas.

Tsukasa Aso, photograph and biography not available at the time of publication.

Masanori Hara, received the Ph.D. degree in science from University of Toyama, Japan, in 2003. He is currently an Associate Professor with the Academic Assembly, Faculty of Science, University of Toyama. His current research interests include measurements of tritium compounds for liquid, solid, and gas phases.

Siriyaporn Sangaroon was born in Phatthalung, Thailand, in 1980. She received the M.S. degree in nuclear technology from Chulalongkorn University, Bangkok, Thailand, in 2005, and the Ph.D. degree in physics from Uppsala University, Uppsala, Sweden, in 2014. She has been with the Department of Physics, Faculty of Science, Mahasarakham University, Maha Sarakham, Thailand, since 2005. She is currently an Associate Professor at Mahasarakham University, a role she has held since 2018. Her research focuses on neutron measurement in magnetically confined fusion plasmas.

Sachie Kusaka, was born in Kyoto, Japan, in 1987. She received the B.S. degree in veterinary medicine from Miyazaki University, Miyazaki, Japan, in 2012, and the Ph.D. degree in engineering from Osaka University, Osaka, Japan, in 2023. She had been working as a clinical veterinarian from 2012 to 2016 and has been involved in a radiation therapy called Boron Neutron Capture Therapy (BNCT) as a technician with Osaka University since 2016. Her

current research interests include the imaging technology for radiation therapy.

Shingo Tamaki, photograph and biography not available at the time of publication.

Isao Murata, was born in Higashiosaka, Osaka, Japan, in 1962. He received the B.S. and M.S. degrees in nuclear engineering from Osaka University, Osaka, Japan, in 1986 and 1988, respectively, and the Ph.D. degree in engineering from Osaka University in 1999. He was engaged in neutronics and shielding design study for high temperature gas-cooled reactor (HTGR) in Japan Atomic Energy Research Institute (JAERI) from 1988 to 1994. From 1995, he had been carrying out fusion neutronics studies in Osaka University and started basic research for boron neutron capture therapy (BNCT) from 2002. From 2001 to 2003, he stayed in Forschungszentrum Juelich, Germany to perform theoretical study for Monte Carlo transport code for the European Spallation Source (ESS) target design. He is currently involved in neutronics studies for fusion reactor and BNCT. He has been a professor in Osaka University since 2014. His current research interests include neutron backscattering reaction cross section for fusion reactor design and separate measurement of neutron and gamma-ray in a mixed field of neutron and gamma-ray in BNCT.

Sho Toyama, photograph and biography not available at the time of publication.

Misako Miwa, photograph and biography not available at the time of publication.

Shigeo Matsuyama, photograph and biography not available at the time of publication.

Masaki Osakabe, photograph and biography not available at the time of publication.